Fast *in vivo* imaging of SHG nanoprobes with multiphoton light-sheet microscopy

Guy Malkinson‡, Pierre Mahou‡, Élodie Chaudan, Thierry Gacoin, Ali Y. Sonay, Periklis Pantazis, Emmanuel Beaurepaire, and Willy Supatto

‡ These authors contributed equally to this work.

SUPPORTING INFORMATION

11 pages

5 Supporting Figures (Figure S1-S5)

4 Supporting Movies (Movie 1-4)

2 Supporting Results

FIGURE S1

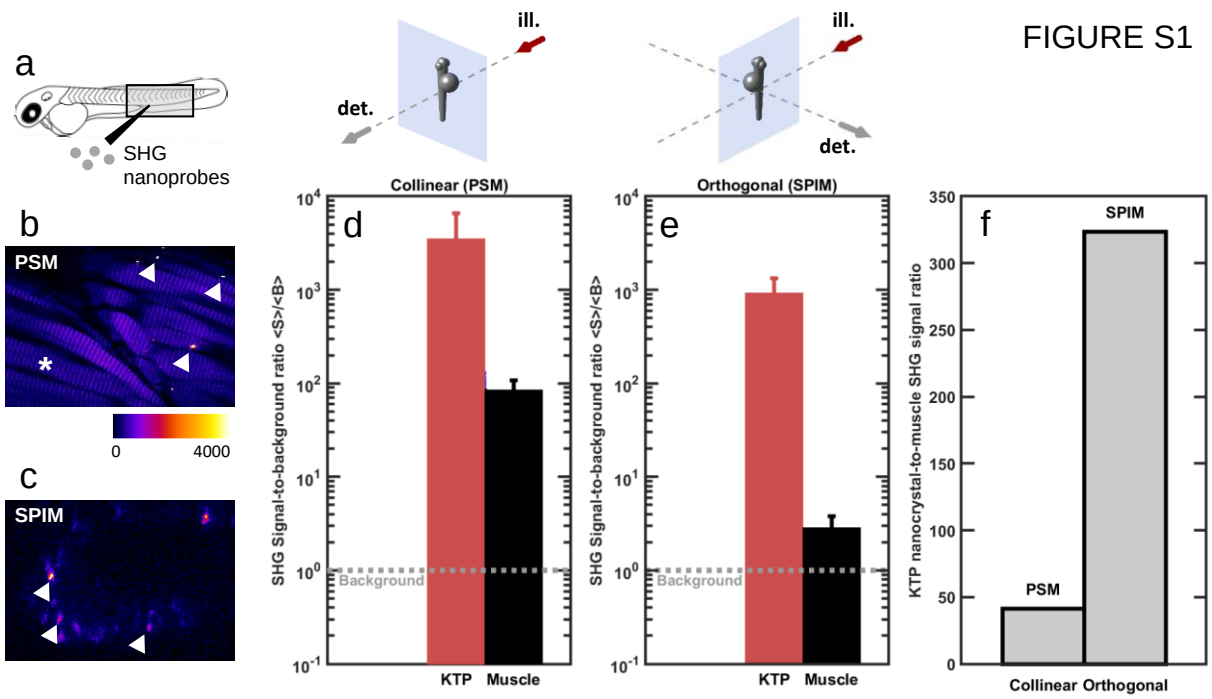

Figure S1. Comparison of SHG detection efficiency using orthogonal (SPIM) or collinear (PSM) geometry to image SHG nanocrystals or endogenous sources of SHG. (a) KTP nanocrystals were injected to the zebrafish embryo tail muscle. (b-c) Single z-stacks of a zebrafish embryo were taken in collinear (b) and orthogonal (c) geometry. SHG signals generated by the skeletal muscle, seen as vertical striations, were detected only using PSM (b), whereas signals from SHG nanoprobes, seen as small localized points (white arrows) were detected in both cases (b-c). (d-f) Quantification of the data shown in (b-c), respectively. For each type of geometry, the mean intensity values through the 3D z-stack are given for the KTP nanocrystals (red) and for muscle region (black). Note that in the orthogonal geometry (c and e), The SHG signals from muscle were hardly visible and only slightly above the background level (gray dotted line). The KTP nanocrystal-to-muscle SHG signal ratio (f) obtained from these measurements showed a pronounced difference between collinear and orthogonal geometry: when using PSM imaging as a reference, SHG signals from KTP nanocrystals were an order of magnitude more efficiently detected than signals from muscles using SPIM. ill., illumination; det. detection.

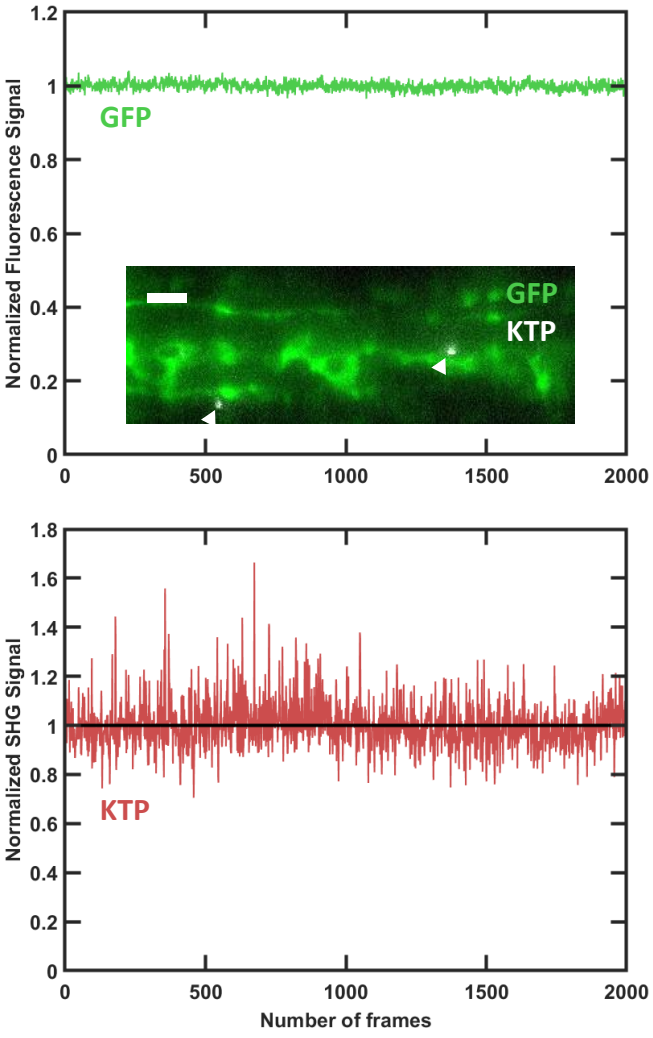

FIGURE S2

Figure S2. Photostability of fluorescence and SHG signals during multimodal multiphoton *in vivo* imaging. Graphs of fluorescence signals from GFP (green, top) and SHG signals from KTP (red, bottom) normalized to the mean depending the number of acquired frames during multimodal multiphoton imaging (inset, fluorescence signal in green and KTP nanocrystals in gray indicated with white arrowheads, scale bar 20 µm). Image acquired at 75 fps, 10 ms exposure time, 930 nm illumination wavelength and 150 mW mean power.

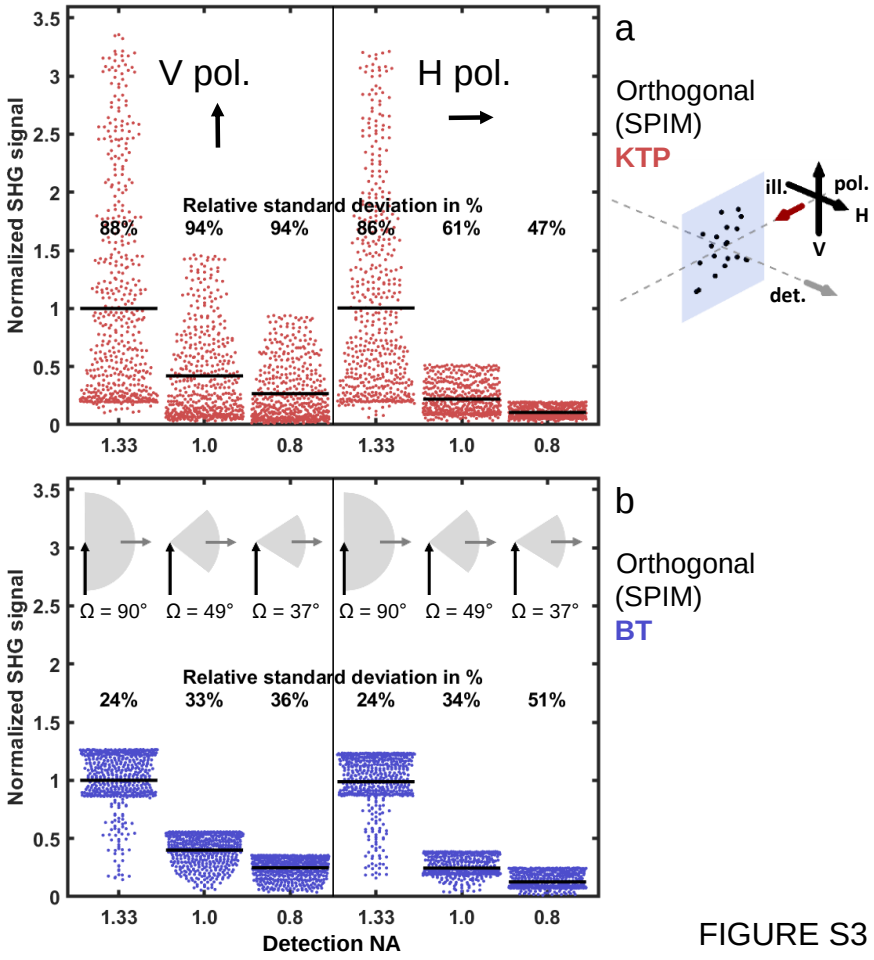

FIGURE S3

Figure S3. Simulation of SHG signals detected from individual KTP and BT nanocrystals depending on detection numerical aperture (NA). Simulation of SHG signal distributions from 500 KTP (a, red) and BT (b, blue) nanocrystals using linear vertical (V, left) or linear horizontal (H, right) polarization of the illumination light in orthogonal geometry of SPIM. Distributions are plotted depending on the detection NA (0.8, 1.0 or 1.33 values, corresponding to 90, 49 and 37° semi-cone angle Ω of detection). Random distribution of nanocrystal orientations results in spreading of signal levels around the mean (black horizontal lines). Signal for each polarization is normalized to the signal mean in the 1.33 detection NA case. Note: NA=1.33 corresponds to the total radiated SHG signal and can be directly compared to PSM. The 24% relative standard deviation in the case of BT is consistent with previous work obtained in PSM[39]. Signal mean and relative standard deviation are indicated for 10,000 nanocrystals simulated with random orientations.

FIGURE S4

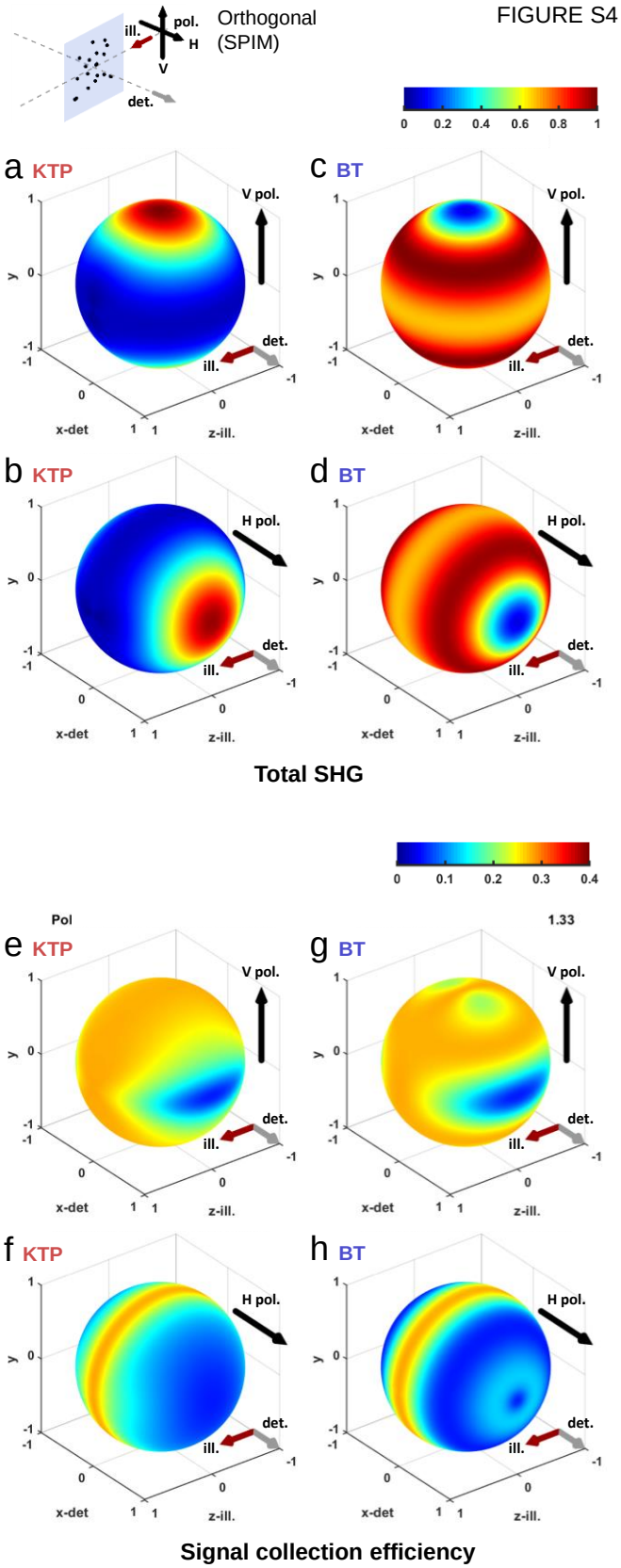
Orthogonal
(SPIM)
ill.
pol.
H
V
det.
0 0.2 0.4 0.6 0.8 1
a KTP
c BT
b KTP
d BT
V pol.
H pol.
det.
ill.
x-det
z-ill.
Total SHG
0 0.1 0.2 0.3 0.4
Pol
1.33
e KTP
g BT
f KTP
h BT
Signal collection efficiency

Figure S4. Simulation of total SHG generated and signal collection efficiency depending on KTP and BT nanocrystal orientation and linear polarization of the illumination light in light-sheet microscopy. (a-d) Simulation of signal intensity distribution for all possible nanocrystal orientations for KTP (a-b) and BT (c-d) nanocrystals using vertical (a and c) or horizontal (b and d) linear polarization in SPIM with a 1.33 detection NA. Signals were calculated, displayed and normalized the same way as Figure 4d-g, except for the detection NA value. The plot corresponds to the distribution of the total SHG signal radiated by the nanoprobes. While KTP nanocrystals behave as a single dipole, the BT nanocrystal radiates a constant signal almost independently on its 3D orientation. (e-h) signal collection efficiency is estimated by computing the ratio of simulations using a 0.8 (Figure 4d-g) and a 1.33 (a-d) detection NA before signal normalization. These graphs show that using a H-polarization result in a poor signal collection efficiency when using SPIM for almost all nanocrystal orientations. Red and gray arrows corresponds to the SPIM illumination and detection axes, respectively. Represented signal is a spline interpolation of signals from 4,000 nanocrystals simulated with random orientations. ill., illumination; det. detection; V, vertical; H, horizontal.

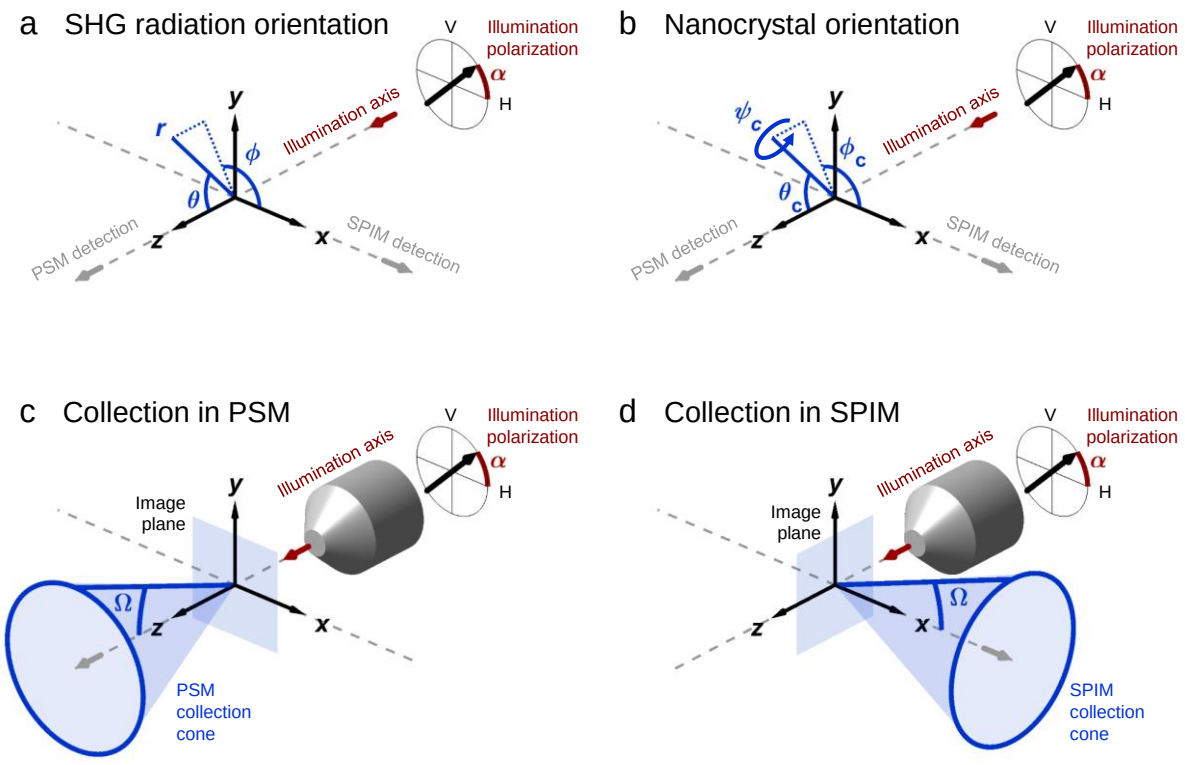

FIGURE S5

Figure S5. Spatial coordinate systems used in simulations. (a) (x,y,z) and (r,θ,φ) are the Cartesian and spherical coordinate system of the laboratory frame, respectively. (b) $(\phi_C, \theta_C, \psi_C)$ are the rotation angles of the nanocrystal defined in the laboratory frame. The semi-cone angle Ω of signal collection is defined in the PSM geometry (c) and in the SPIM geometry (d).

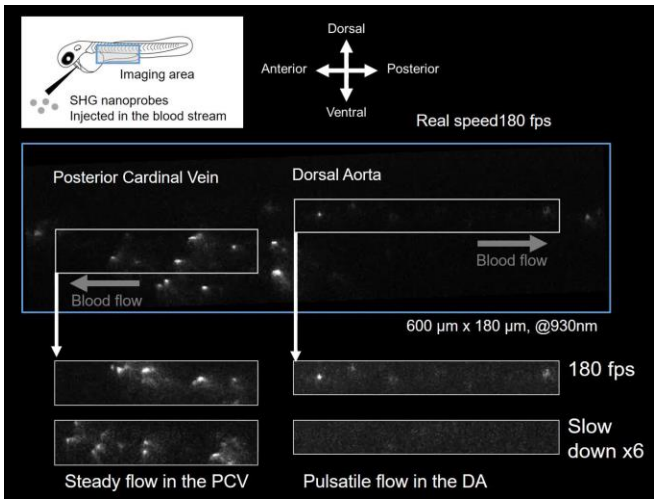

Movie 1. KTP nanocrystals imaged with SHG-SPIM at 180 fps with 2 ms exposure time. A 3 dpf zebrafish embryo was injected with KTP nanocrystals and imaged at an excitation wavelength of 930 nm. KTP nanocrystals flowing from right to left (rostral-to-caudal direction) can be seen in the posterior cardinal vein and flowing from left to right in the dorsal aorta. An area of 600 x 180 μm^2 was imaged at 180 fps, corresponding to >43 MHz pixel rate.

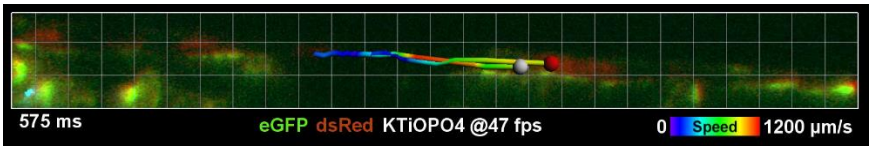

Movie 2. Multimodal *in vivo* imaging combining red and green fluorescence with SHG from nanoprobes. A 2.5dpf zebrafish embryo expressing eGFP in its endothelial cells and dsRed in its red blood cells (RBCs) was injected with KTP nanocrystals in the blood stream and imaged at 47 fps at an illumination wavelength of 930nm. The image sequence was taken in the trunk region and the fast pulsatile movement of RBCs and KTP nanocrystals flowing from left to right (caudal-to-rostral direction) can be seen in the main artery. Simultaneous tracking a red blood cell (red dot) and a SHG nanoprobe (gray dot) moving at different speed and up to 1200µm/s. Grid scale 20 µm.

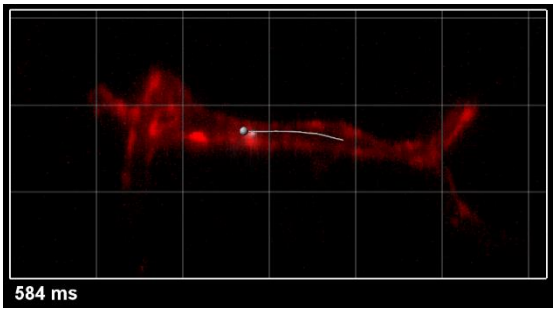

Movie 3. Multimodal *in vivo* imaging combining red fluorescence with SHG from nanoprobes. A 2.5dpf zebrafish embryo expressing mCherry in its endothelial cells was injected with KTP nanocrystals in the blood stream, and imaged at 65 fps at an illumination wavelength of 1060nm. The movie was taken in the brain and show a nanocrystal flowing from the left mesencephalic vein into the left middle cerebral vein. This nanocrystal was tracked (gray dot and track) during 1.7s. At the end, 8 tracks are displayed (30s acquisition) showing nanocrystals flowing from the left or right mesencephalic vein into the left or right middle cerebral vein. Grid scale 50 µm.

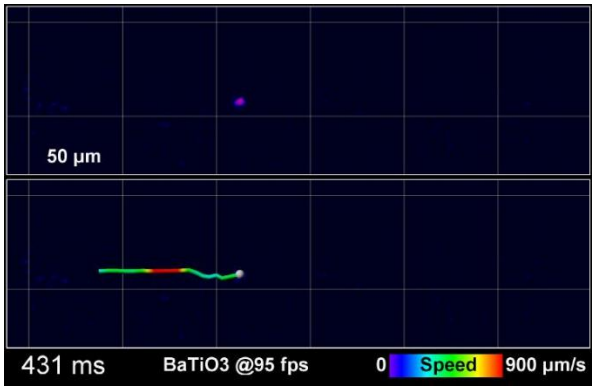

Movie 4. BT nanocrystals imaged with SHG-SPIM at 95 fps with 5 ms exposure time. A 3 dpf zebrafish embryo was injected with BT nanocrystals and imaged at an excitation wavelength of 930 nm. BT nanocrystals flowing from left to right (caudal-to-rostral direction) can be seen in the main vein. Raw images (top) and tracked data (bottom). Color code of the trajectory code for instantaneous speed from 0 (blue) to 900 µm/s (red). Scale grid 50 µm.

Supporting Result 1. Sensitivity to incident polarization of SHG nanoprobes with strongest signals

The sensitivity of SHG signal to incident polarization was investigated in **Figure 3**. While the results from simulations and experiments were very similar in the BT case (plain gray and blue lines in **Figure 3d**), we observed a stronger anisotropy in the experiments than in the simulations in the case of KTP nanocrystals (plain gray and red lines in **Figure 3b**). To identify possible causes for that difference, we plotted the mean signal from the 20% strongest or weakest among the 1000 simulated nanoprobes (doted and dashed gray lines in **Figure 3**, respectively). We note here that since all simulated particles have the same size, the level of detected SHG signals depends only on the $\chi^{(2)}$ tensors (i.e. the nature of the nanocrystals) and on the difference in relative orientation between the nanocrystal and the incident polarization. Interestingly, these two populations, i.e. strongest and weakest signals, exhibited a very different sensitivity to incident polarization, especially in the KTP case (**Figure 3b** and **3d**). Indeed, the KTP nanocrystals with strongest detected signals exhibited a pronounced anisotropy, while the weakest ones did not (0.11 and 0.90 anisotropy factor, respectively). This calculation suggests that the observed difference between experiments and simulations in the KTP case could result from an experimental bias towards measuring mainly nanoprobes with the strongest signals. The difference in sensitivity to incident polarization between weak and strong images of nanoprobes is not as pronounced in the BT case and shows the opposite trend: the BT nanocrystals with strongest detected signals exhibited a lower anisotropy than the weakest ones (0.68 and 0.37 anisotropy factor, respectively).

Supporting Result 2. Detection numerical aperture has effect on both mean and spread of SHG-SPIM signals

To mitigate the spread of SHG signal intensities, we simulated the effect of detection NA ranging from 0.8 to 1.33 in SPIM using KTP or BT nanocrystals with both V- and H-polarization (**Figure S3**). We note that a NA of 1.33 corresponds to a collection of the total radiated SHG from randomly oriented nanoprobes when using a water immersion objective. Our experimental setup used a 0.8 NA detection objective, which can hardly be increased above 1 for practical reasons. As previously reported in the case of BT nanocrystals in PSM [39], we found that increasing the detection NA in SPIM resulted in both an increase in signal mean level and a decrease in relative standard deviation when using a V-polarization, which is beneficial for imaging purposes (**Figure S3**). However, we

noted that the reduction of signal spread was more pronounced for BT than for KTP (comparing **Figure S3a** and **S3b**, left). When using an H-polarization, KTP nanocrystals exhibited a specific behavior: despite a significant decrease in signal mean level, using a low detection NA could result in a lower signal spread (from 86 to 47%, **Figure S3a**, right). In general, SPIM imaging of SHG nanoprobes can be improved by adjusting the detection NA, which has effect on both the signal mean level and its spread as a function of nanoprobe orientation.